Supplementary Note 1: Arrhenius model

To assess chronic reliability, we utilized extrapolations based on Arrhenius scaling of time to failure with temperature. By observing the behavior of devices at elevated temperatures, this scaling approach yields estimates for the time of failure at reduced temperatures. This form of accelerated testing utilizes the Arrhenius equation:

$$r = A \exp(\frac{-E_a}{kT}) \quad (1)$$

where r = rate of the process, A = a proportional multiplier, E_a = the activation energy for the process, and k = Boltzmann constant.

Rearranging the equation yields a model for the temperature dependence of the failure time,

$$\ln\left(\frac{t_2}{t_1}\right) = \frac{E_a}{k}\left(\frac{1}{T_2} - \frac{1}{T_1}\right) \quad (2)$$

where t_1 = time to failure at T_1 and t_2 = time to failure at T_2.

For T_1 = 90 ℃, T_2 = 60 ℃, experiments show that t_1 = 6 days and t_1 = 30 days. From these data, the value of E_a can be determined to be 60 kJ/(mol.K), similar to values in the literature [1]. This information allows extrapolation to time to failure at 37 ℃, which is 180 days (6 months).

Supplementary Note 2: Tailored properties in stretchable multi-channel antennas

Stretchable multi-channel antennas can be designed with a wide range of operating frequencies. **Supplementary Fig. 5** explains the process of selecting designs that define a desired pair of operational frequency (and, therefore, channel separation). In these examples, the operation frequency at Channel 2 varies from 2.7 to 3.1 GHz with a frequency of 2.3 GHz at Channel 1. The total capacitance required for resonance at the corresponding frequency ranges appears in **Supplementary Fig. 5**. This capacitance provides an estimate of the dimensions of the antenna. Based on the estimates and unit capacitances in **Fig. 4D**, it is possible to determine the number of serpentine pairs needed for resonance at the operation frequency.

Supplementary Note 3: Calculation of electrostatic potential and capacitance

Assume that the length in the X-direction is much greater than the height in the Y-direction. The boundary function of the serpentine lines can be expressed by,

$$y = h - lcos(kx) \quad \text{where } k = \frac{2\pi}{p} \tag{3}$$

The electrostatic potential function, $\Psi(x, y)$, satisfies the boundary and periodic conditions given by,

$$\Psi(x, y) = \begin{cases} V_0 & if\ y = h - lcos(kx) \\ -V_0 & if\ y = -h + lcos(kx) \end{cases} \tag{4}$$

$$\Psi(x, y) = \Psi(x + p, y) \tag{5}$$

Based on these conditions, one can solve Laplace equation,

$$\frac{\delta^2\Psi(x,y)}{\delta x^2} + \frac{\delta^2\Psi(x,y)}{\delta y^2} = 0 \tag{6}$$

beginning with a general solution that exploits separation of variables.

$$\Psi(x, y) = X(x)Y(y) \tag{7}$$

Plugging the (7) into (6) and imposing the conditions in (4) and (5) leads to

$$X_n(x) = a_n cos(nkx) + b_n sin(nkx) \qquad n = 1,2,3, \ldots \tag{8}$$

$$Y_n(y) = c_n\, e^{nky} + d_n e^{-nky} \qquad n = 1,2,3, \ldots \tag{9}$$

$$acos(qx) + bsin(qx) = acos(q(x + p)) + bsin(q(x + p))$$

$$\text{where } q, p = 2\pi n,\ n = 1,2,3,\ldots \tag{10}$$

$$\Psi_n(x, y) = \left(a_n cos(nkx) + b_n sin(nkx)\right)[c_n\, e^{nky} + d_n e^{-nky}],$$

$$n = 1,2,3, \ldots \tag{11}$$

$$\Psi(x,y) = \frac{V_0}{h}\, y + \frac{V_0}{h}\, \frac{sinh(ky)\, cos(kx)}{sinh(k(h - l\, cos(kx)))} \qquad k = \frac{2\pi}{p} \tag{12}$$

The derivative of this expression with respect to y yields the Y components of the electric field,

$$\mathrm{E}_Y(x,y) = -\frac{V_0}{h} - \frac{V_0}{h}\, k\, \frac{cosh(ky)\, cos(kx)}{sinh(k(h - l\, cos(kx)))} \qquad k = \frac{2\pi}{p} \tag{13}$$

Next, we calculate the capacitance between two serpentine lines. This serpentine shaped- capacitor consists of infinite capacitors where capacitance is determined by (**Fig. 4B**),

$$dC = \varepsilon \frac{dx}{y} \qquad \text{where } y = 2h + 2\, l sin\, x \tag{14}$$

Integrating this expression along the length of the serpentine lines yields the capacitance.

$$C = \int dC = \int \frac{dx}{y} = \int \frac{dx}{2h + 2\, l sin\, x} \tag{15}$$

Supplementary Note 4: MATLAB code for motion tracking algorithm

```
vidDevice = imaq.VideoDevice('winvideo', 1, 'YUY2_320x240', ...
'ROI', [1 1 320 240], ...
'ReturnedColorSpace', 'rgb');
optical = vision.OpticalFlow('OutputValue', 'Horizontal and vertical components in complex form');
maxWidth = imaqhwinfo(vidDevice,'MaxWidth');
maxHeight = imaqhwinfo(vidDevice,'MaxHeight');
shapes = vision.ShapeInserter;
shapes.Shape = 'Lines';
shapes.BorderColor = 'Custom';
shapes.CustomBorderColor = [255 0 0];
r = 1:20:maxHeight;
c = 1:20:maxWidth;
[Y, X] = meshgrid(c,r);
hVideoIn = vision.VideoPlayer;
hVideoIn.Name = 'Original Video';
hVideoIn.Position = [30 100 320 240];
hVideoOut = vision.VideoPlayer;
hVideoOut.Name = 'Motion Detected Video';
hVideoOut.Position = [400 100 320 240];
nFrames = 0;
```

```
devices = daq.getDevices;
devices(1);
s = daq.createSession('ni');
addDigitalChannel(s,'Dev1','port0/line0:3','OutputOnly');
outputSingleScan(s,[ 1 1 1 1]);
sum=0;
while (nFrames < 2000)
rgbData = step(vidDevice);
optFlow = step(optical,rgb2gray(rgbData));
optFlow_DS = optFlow(r, c);
H = imag(optFlow_DS)*50;
V = real(optFlow_DS)*50;
lines = [Y(:)'; X(:)'; Y(:)'+V(:)'; X(:)'+H(:)'];
rgb_Out = step(shapes, rgbData, lines');
%%rgb_Out = step(shapes, rgb_Out, lines');
%%step(hVideoIn, rgbData);
step(hVideoOut, rgb_Out);
x=rgbData-rgb_Out;
for i=1:1:240
   for j=1:1:320
         if (x(i,j,3) > 0)
            if (j >160)
            outputSingleScan(s,[ 0 0 0 0]);
                  i=240;
                              j=320;
            else
              outputSingleScan(s,[ 1 1 1 1]);
                  i=240;
           j=320;
            end
      end
   end
end

nFrames = nFrames + 1;
end
release(hVideoOut);
release(hVideoIn);
release(vidDevice);
```

Reference

1. Thomas, T. H. & Kendrick, T.C. Thermal Analysis of Polydimethylsiloxanes. I. Thermal Degradation in Controlled Atmospheres. *J.Polym. Sci*. 7, 537-549 (1969).

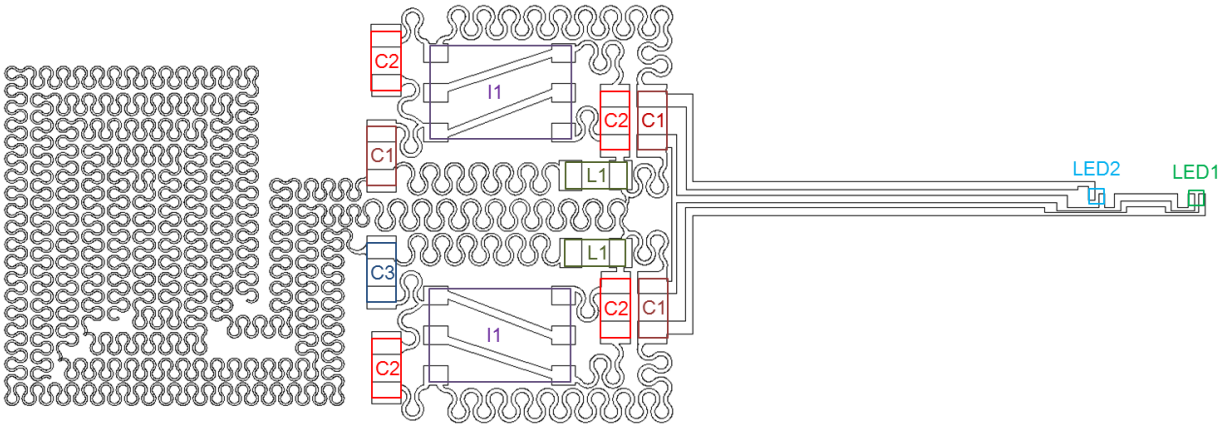

	Components	**Product number**	**Vendor information**
LED1	540 nm, 0.22 mm x 0.27 mm x 0.05 mm	C527TR2227-0215	Cree Inc.
LED2	465 nm, 0.22 mm x 0.27 mm x 0.05 mm	C460TR2227-0216	Cree Inc.
C1	Capacitor, 1 pF, 0.2 mm x 0.4 mm x 0.22 mm	250R05L1R0BV4T	Johanson Technology
C2	Capacitor, 5 pF, 0.6 mm x 0.3 mm x 0.33 mm	250R05L5R1CV4T	Johanson Technology
C3	Capacitor, 3 pF, 0.6 mm x 0.3 mm x 0.33 mm	250R05L3R1CV4T	Johanson Technology
I1	Schottky diode, 1.7 mm x 1.5 mm x 0.5 mm	1PS66SB82,115	NXP Semiconductor
L1	Inductor, 2.7 nH, 0.2 mm x 0.4 mm x 0.22 mm	L-05B2N7SV6T	Johanson Technology

Supplementary Fig. 1. Layout and component information for the multi-channel devices.

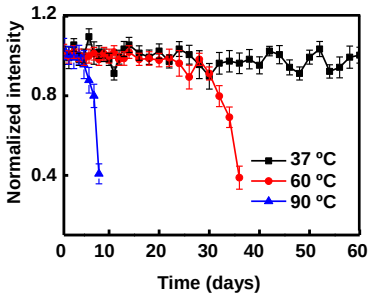

Supplementary Fig. 2. Assessment of variations in normalized light intensity produced by the multi-channel system as a function of time of immersion in physiological PBS (7.4 pH) solution at three different temperatures.

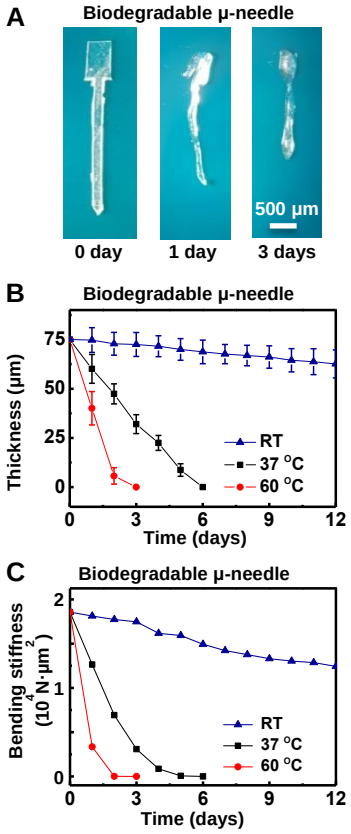

Supplementary Fig. 3. (A) Images of a biodegradable, injectable μ-needle in physiological PBS solution after 0 day (left), 1 day (middle), and 3 days (right) respectively. Results of measurements of the μ-needle thickness (B) and bending stiffness (C) as a function of time of immersion in PBS at a variety of temperatures.

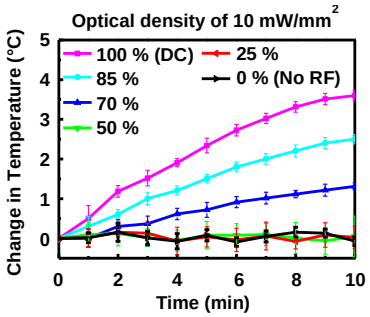

Supplementary Fig. 4. In vivo monitoring of temperature of a mouse during device operation, for various duty cycles (DC).

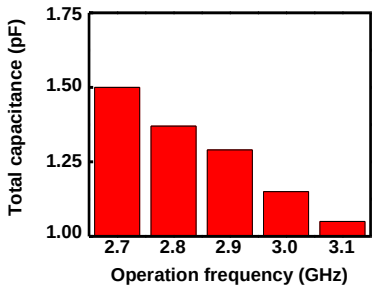

Supplementary Fig. 5. Total capacitance values for stretchable antennas with resonance frequencies between 2.7 to 3.1 GHz .

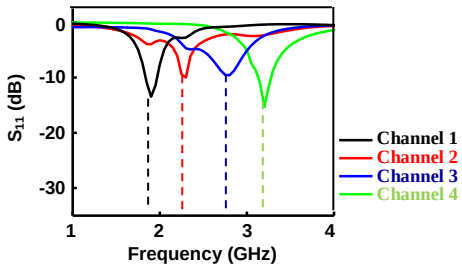

Supplementary Fig. 6. Scattering coefficients, S_{11}, of a 4-channel stretchable antenna. The antenna has 4 operation channels at a frequency of 1.9 (black), 2.2 (red), 2.8 (blue), and 3.2 (green) GHz, respectively.

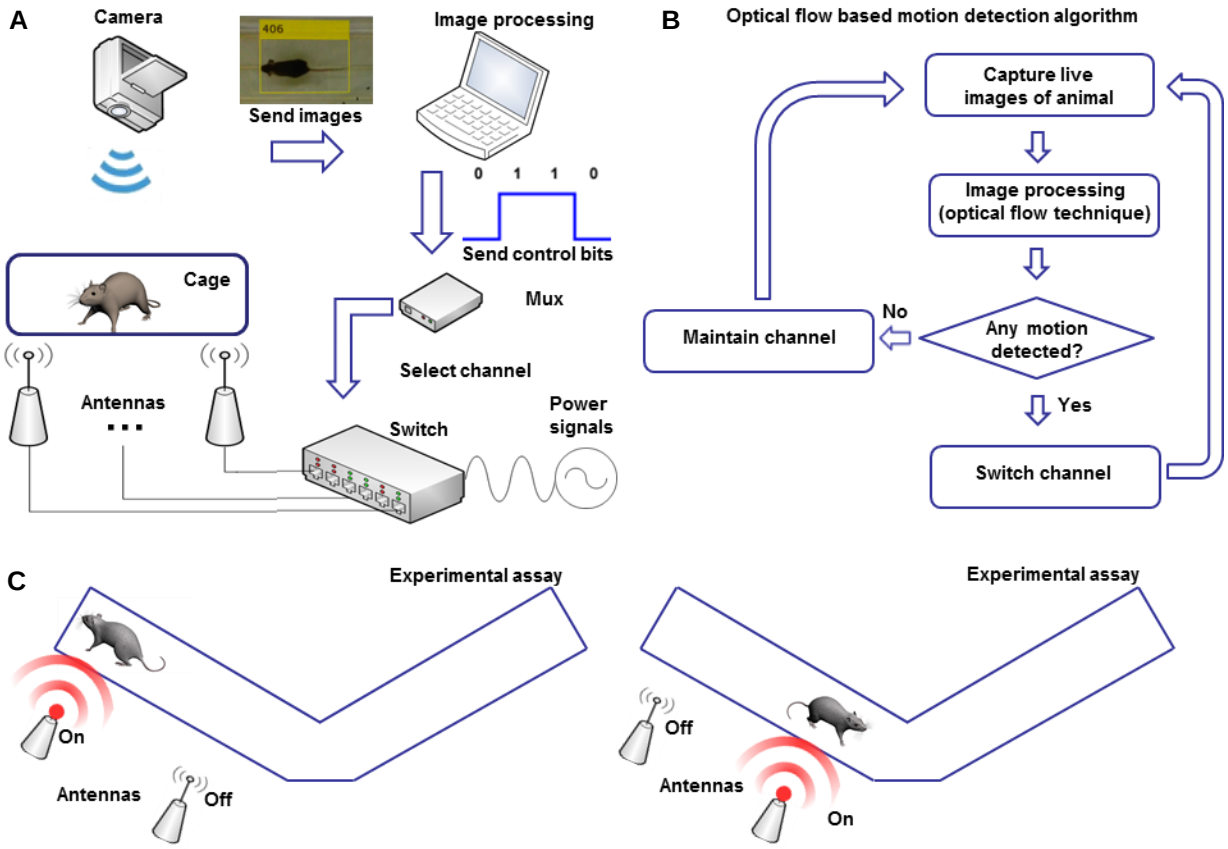

Supplementary Fig. 7. (A) Illustration of motion tracking power transmission systems. A camera monitors the location of a mouse and sends images to the base station, which processes the images and sends control signals to the multiplexer (Mux). Output signals from Mux manipulate a switch that activates the appropriate circuit to transmit power with the appropriate antenna. These processes occur within 1 ms which is fast enough to respond to the motions of a mouse instantaneously. (B) Flowchart of the motion detection algorithm. (C) Illustration of smart power transmission. The antenna that is closest to the mouse is enabled and transmits power.

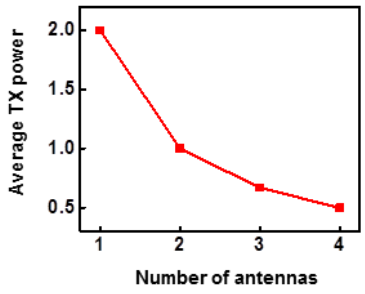

Supplementary Fig. 8. Plot of average TX power as a function of number of antennas. The smart power system distributes a given TX power of 2 W across the antennas.

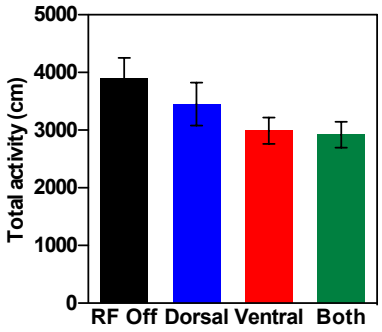

Supplementary Fig. 9. Analysis of the total distance traveled, as an assessment of activity level, during a 20 min experiment.

Process	**Purpose**	**Required time for 5 devices**	**Equipment**	**Progress level (%)**
1. Preparation of PMMA coated glass	Sampling for transfer	0.5 hour	Cleanroom Spin-coater	5
2. PI film fabrication	Bottom encapsulating layer	1.5 hours	Cleanroom, Vacuum oven	15
3. Metal (Ti/Au) deposition	Interconnection	1.5 hours	E-beam deposition	25
4. Metal patterning		1 hours	Cleanroom, Mask aligner	30
5. PI encapsulation	Top encapsulating layer	1.5 hours	Cleanroom, Vacuum oven	40
6. PI/Metal/PI patterning	Patterning for stretchable circuits	1 hours	Cleanroom, mask aligner,	50
7. PI etching		1.5 hours	RIE	60
6. Components transfer	Active components integration	2.5 hours	Solder, Microscope	80
7. PDMS encapsulation	System packaging	0.5 hour	Oven	100

Supplementary Table 1: Fabrication process details

Supplementary Movie 1. Video of an operating device. This demonstrates that the frequency of the incident RF radiation can be adjusted to activate the channels independently.

Supplementary Movie 2. Video of a freely behaving animal with the device implanted in a cage. This demonstrates that wireless power transmission systems can enable continuous operation throughout a location of interest.